

Short Communication

An Investigation of the Surface Quality and Corrosion Resistance of Laser Remelted and Extreme High-Speed Laser Cladded Ni-based Alloy Coating

Ming-Xia Liu^{1,2,*}, Zhao Li¹, Geng-Rong Chang¹, Zhi-Fu Yin¹, Xiu-Ping Zhang², Yu Meng¹, Yang-Yang Xu³, Fei Ma³, and Ke-Wei Xu^{1,3}

¹Shaanxi Key Laboratory of Surface Engineering and Remanufacturing, Xi'an University, Xi'an 710065, China

²Xi'an Key Laboratory of prototyping and optimization of implantable devices, Xi'an University, Xi'an, 710065, China

³State Key Laboratory for Mechanical Behavior of Materials, Xi'an Jiaotong University, Xi'an 710049, China

*E-mail: liumingxia1121@163.com

Received: 6 January 2022 / Accepted: 22 February 2022 / Published: 5 April 2022

Ni-based coatings are prepared on 2Cr13 steel substrate by extreme high-speed laser cladding and subsequent laser remelting (EHLA-LR). The effects of laser remelting (LR) treatment on the morphology, microstructure, residual stress and corrosion resistance of extreme high-speed laser cladded (EHLA) coatings are investigated in details. The results demonstrate that the integrated EHLA-LR process could dramatically reduce the surface roughness by 86%, improve the surface compactness and optimize the surface flatness. The dendrite spacing in the near surface region of the coating via EHLA-LR decreases with refined grains, while the phases of the coatings change little in spite of LR treatment. It was found that the residual compressive stress of the coatings is maintained, but it is slightly reduced upon LR. Furthermore the coatings via EHLA-LR possess better corrosion resistance than that of coatings via EHLA owing to the increased surface compactness and grain refinement by LR process.

Keywords: Extreme high-speed laser cladding; Laser remelting; Microstructure; Grain refinement; Residual stress; Corrosion resistance

1. INTRODUCTION

Among laser cladding (LC) technologies, extreme high-speed laser cladding (EHLA) has aroused more and more attentions since its invention in 2017. EHLA exhibits many technical characteristics of low heat input, high deposition efficiency, low dilution rate and simple post-treatment procedures [1,2].

The coating quality could be efficiently improved by adjusting the relative positions of laser, powder and molten pool, optimizing the melting form and energy absorption ratio of powder. Moreover, EHLA as an environment-friendly technique has enormous potentials to replace hard chrome electroplating and spraying methods [3-5], in the strategic fields, such as, turbine rotor, drive shaft, piston rod and other rotating components. Nevertheless, the poor surface flatness of EHLA coatings will affect the aerodynamic performances of rotating parts, and fine grinding will reduce the effective coating. Accordingly, it is urgent to explore the appropriate hybrid process to improve the surface quality of coatings via EHLA.

Laser remelting (LR) is proposed to enhance the properties of coatings themselves without any additional materials [6-8]. Essentially, LR could not only eliminate the original defects, such as, pores, cracks and inclusions, but also improve the hardness, wear resistance and corrosion resistance through quench recrystallization. Accordingly, it has been extensively combined LR with other spraying techniques, such as, supersonic flame spraying (HVOF) [9,10], plasma spraying [11], cold spraying [12] and flame spraying [13]. Recently, a combination between LR and cladding becomes one of research hotspots. Kawakami et al. [14] and Karmakar et al. [15] found that the surface hardness and high-temperature wear resistance of the steel could be effectively improved, especially for the material with low hardenability. Xu et al. [16] and Lou et al. [17] investigated the microstructure and corrosion behavior of Fe-based coatings prepared by an integrated process of EHLA and LR (EHLA-LR for short). Their studies exhibited that the coating possessed better corrosion resistance owing to the new formed stable oxide film and the gradually disappeared granular characteristics on the surface of the cladding coating. Deng et al. demonstrated the effect of laser cladding and laser remelting (LC-LR) composite process on the residual stress of 316L stainless steel cladding layer [18]. Shi et al. reported the effects of LC-LR on interfacial macrosegregation and exhibited the improved microstructure and microhardness of laser additive manufactured H13/IN625 bimetals [19]. The laser melting+remelting strategy effects the migration of H13 into IN625 molten pools in a layer-by-layer manner, which could result in a cellular-columnar-cellular microstructure transition and the microhardness values with varying standard deviations across the H13/IN625 interface. In another recent work Hwang et al. analyzed the effect of underwater LR on the quality of selective laser melted (SLM) titanium alloy and reported its hardness was significantly increased after remelting due to the increased heat dissipation and cooling rate in water [20]. To reduce the void level of a component fabricated via directed energy deposition with laser (DED-L), Paes et al. investigated the forming quality of iron and IN625 materials post-treated by LR and exhibited that most of the voids originating from the DED-L process could be effectively mitigated [21]. In the engineering applications, the integrated process of LC-LR has been used to repair the turbine engine blades [22].

Apparently, the integrated technology EHLA-LR exhibits great potential applications as preparing high-quality coatings to protect the rotating parts. Although nickel-based alloy has good corrosion resistance, high strength and plastic toughness [19,23-25], the fabrication of Ni-based alloy on stainless steel by using EHLA-LR still remains challenging. In this work, IN625 corrosion-resistant coatings were prepared on 2Cr13 steel substrate via EHLA, and then LR post-treatment was carried out. The morphology, microstructure, residual stress and corrosion resistance of the coatings before and after remelting treatment were investigated.

2. EXPERIMENTAL DETAILS

2.1 Materials and Coating Preparation

2Cr13 steel with 120 mm×120 mm×20 mm in size is used as the cladding substrate. Table 1 lists its composition. Prior to the laser cladding, the surfaces of the substrates are sandblasted and then ultrasonic cleaned in absolute ethanol to remove the oxides. Subsequently, the surface modification on 2Cr13 steel is carried out in two different processes, viz. the extreme high-speed laser cladding (EHLA), the integrated process of extreme high-speed laser cladding and laser remelting (EHLA-LR). In the laser cladding process, the powder feedstock is IN625 nickel-based alloy with the particle size of 50~100 μm. Table 2 lists the composition of IN625 alloy powder. Before cladding, the powder is dried in vacuum at 200 °C for 2 hours to remove moisture.

Table 1. Chemical composition of 2Cr13 steel substrate material (wt.%)

Element	C	Si	Mn	S	P	Cr	Cu	Ni	Fe
Content	0.19	0.28	0.20	0.007	0.028	12.65	0.11	0.12	Bal.

Table 2. Chemical composition of Ni-based alloy powder (wt.%)

Element	C	Al	Ti	Fe	Mo	Nb	Cr	Ni
Content	~0.1	0.1~0.2	0.1~0.3	2.5~3.5	8.0~10.0	3.0~4.0	18.0~25.0	Bal.

A fiber laser (model ZKZM-4000) integrated with a five-axis CNC workstation was used to prepare the specimens.

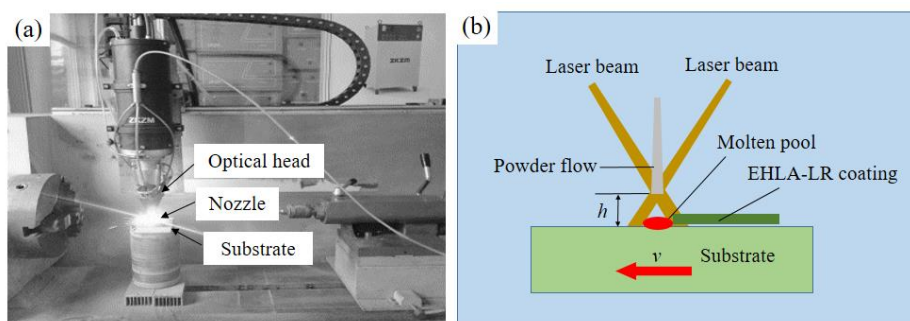


Figure 1. The EHLA and LR equipment (model ZKZM-4000) used in the present study: (a) Physical picture; (b) Schematic diagram of Ni-based alloy coating on 2Cr13 steel substrate via EHLA-LR, while the laser scanning direction was the same as the cladding direction.

The EHLA and LR equipments and experiments with synchronous powder feeding are illustrated in Figure 1. Detailed conditions of EHLA and LR cladding processes are shown in Table 3. LR treatment was applied on the coating after cladding for comparison. In case of remelting, the process parameters were selected in order to achieve appreciable depth of hardened layer. Based on the inherent laser-material interaction characteristics of the two processes, different laser power parameters for laser remelting and cladding were chosen. The melting pool was protected by N₂ gas during cladding. In remelting processing, the laser scanning direction was the same as the cladding direction.

Table 3. Processing parameters used in extreme high-speed laser cladding (EHLA) and laser remelting (LR)

Parameters	Value	
	EHLA	LR
Laser Power (P , kW)	1600	1000
Scanning speeding (V , m/min)	7	7
Overlapping ratio (R)	60%	60%
Power feeding rate (V_p , g/min)	26	0
Gas flow rate (R_g , L/min)	10	10

2.2 Material Characterization and Performance Test

The surface topography of the EHLA and EHLA-LR specimens is observed by visual measurement. The surface roughness R_a is measured by surface roughness tester (model TIME3221), and ten measurements are averaged for each sample. Three-dimensional microscope (model HIROX KH-1300) and scanning electron microscopy (model Nova Nano SEM 450) are used to observe the cross-sectional morphology of the coatings. HCl: HNO₃=3:1 etchant is used for metallographic sample preparation. The etching time is 5 min. The phases of the coatings are analyzed using 7000S X-ray diffractometer (CuK α , 40 kV voltage and 40 mA current) in scanning angle from 10° to 90°.

After electropolishing pretreatment on the surface of the coatings, the residual stress is measured by X-ray stress diffractometer (model X-350A) with CrK α radiation operated at 20 kV and 5 mA. Residual stress is determined by the traditional $\sin^2\psi$ method with ψ of 0°, 24.2°, 35.3° and 45°. The (220) plane of the Ni-based alloy coatings, corresponding to the 2θ and stress constant k of 128.78° and -675 MPa, respectively, is used in the stress measurement and analysis.

2Cr13 substrate and the coatings via EHLA and EHLA-LR are cut into circular specimens with the diameter of 25 mm and the thickness of 5 mm using a wire EDM system (model HB400). The 200#~1500# sandpapers are adopted to polish the sample surface. Then, the polarization curves of the specimens are measured in 3.5 wt% neutral NaCl solution at room temperature by electrochemical workstation (model CS350). The polarization curves are measured by use of the potentiodynamic polarization tests with the scanning rate of 1 mV/s. The neutral salt spray test is carried out in SHTH-

270 salt spray test chamber at 35 °C for 96 h. An electronic balance with an accuracy of 0.1mg is used to measure the mass loss of the specimens.

3. RESULTS AND DISCUSSION

3.1 Morphology Observation

Figure 2 exhibits surface morphologies and average surface roughness R_a of the coatings. As shown in Figure 2(a), similar to sprayed coatings, the surface of the coating via EHLA is smooth and better than that produced by conventional laser cladding [1, 3]. As shown in Figure 2(b), the surface of the coating via EHLA-LR with metallic luster becomes more compact without cracks, pores and tumour defects. As illustrated in Figure 2(c), upon LR the surface roughness of the EHLA coatings ($13.27 \mu\text{m}$) is substantially reduced down to $1.76 \mu\text{m}$ by 86.7%. That is, LR treatment could improve the surface quality of EHLA coatings effectively. The surface roughness of cladding coating via LR has also been investigated in some literatures [7,16]. As a result, improving the surface roughness could reduce mechanical vibration and increase the service life of workpiece material by post-treated using LR [22].

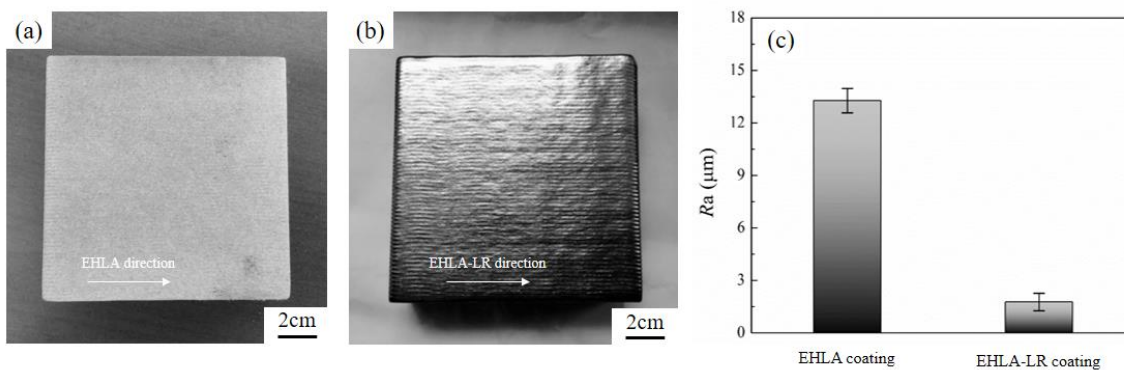


Figure 2. Surface macroscopic morphologies of Ni-based alloy coatings via (a) EHLA, (b) EHLA-LR and (c) average surface roughness R_a values.

Figure 3 shows the cross-sectional macroscopic morphologies of the EHLA and EHLA-LR specimens. It is proved that the surface of the Ni-based alloy cladding layer via EHLA becomes smooth and uniform upon LR, accompanied with compact texture and good metallurgical bond with the substrate. As a result, the thickness of the coatings is reduced from $\sim 0.5 \text{ mm}$ down to $\sim 0.4 \text{ mm}$ by 20%. The dilution ratio of the coating is only 3.4%, that is, high speed laser cladding affect the substrate little.

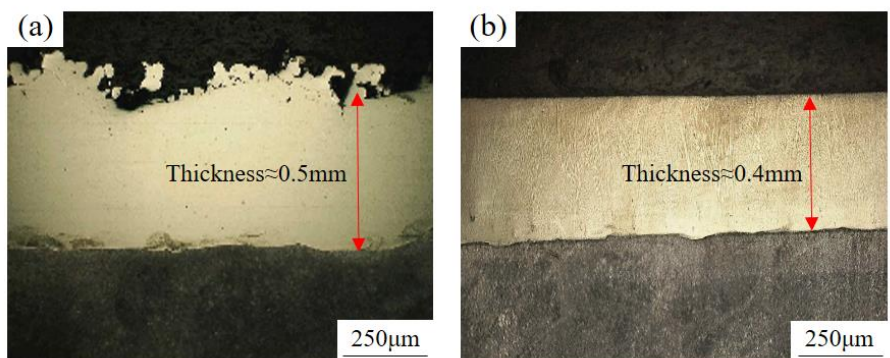


Figure 3. Cross-sectional macroscopic morphologies of Ni-based alloy coatings via (a) EHLA and (b) EHLA-LR.

Figure 4 shows the cross-section images at different position before and after LR. As illustrated in Figures 4(a), before LR, spatters and un-melted powders are observed on the sample surface. Powder splashing results from the instable molten pool, in which heat flow in laser cladding, melting metal powder and rapid cooling are involved. Part of the molten metal flows out of the melting pool and generate splash before solidification, leading to rough surface. Meanwhile, the un-melted powders are adhered on the surface during solidification of molten pool. As shown in Figure 4(d), the splashing of melt drops and un-melted powders are evidently reduced upon LR, as a result, the flatness and compactness of the cladding layer are improved.

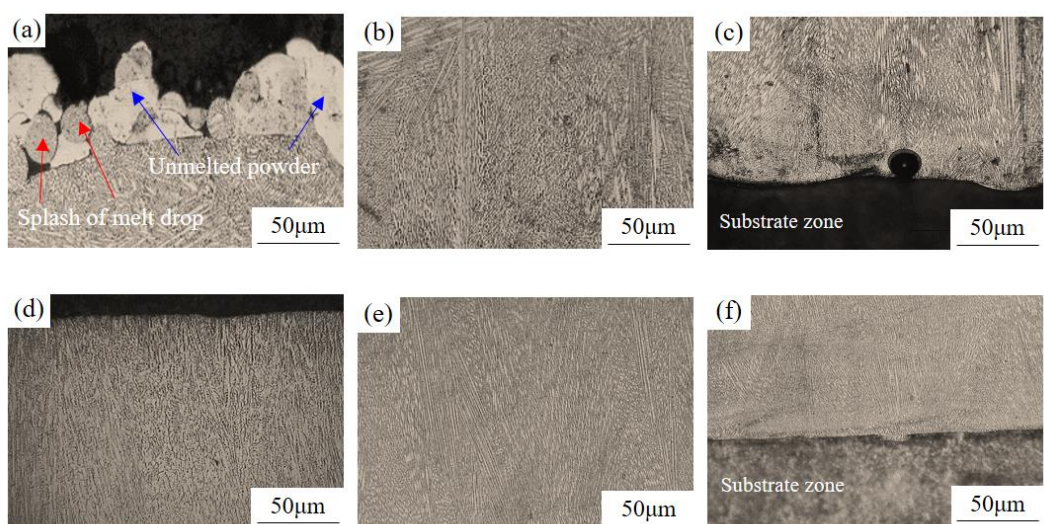


Figure 4. Microstructures in different areas of Ni-based alloy coatings via (a~c) EHLA and (d~f) EHLA-LR: (a,d) top, (b,e) middle, and (c,f) bottom.

Figure 4(a)~4(c) display the microstructures of the near surface, middle and bottom of the coating before remelting. Apparently, the dendrites grow from the bonding zone to the near surface zone. Essentially, a small molten pool is formed in the cladding process, and the fast cooling rate leads to

shortened solute diffusion time and rapid non-equilibrium solidification, as well as dendrite morphology. The columnar dendritic microstructure is dominated by the heat flow. Figure 4(d)~4(f) show the microstructures at the near surface, middle and bottom of the coatings via EHLA-LR. The dendrites are still maintained, but the macrostructure and microstructure at the near surface change considerably.

Figure 5 shows the detailed SEM images of cross-section morphologies at near-surface of the EHLA-LR specimens. Figure 5(a) displays the cross-section SEM image of the cladding layer. Figure 5(b) and 5(c) shows the enlarged microstructures at the near-surface region. As shown in Figure 5(b), the dendrites grow in the opposite direction of heat flow, because the better thermal conductivity near the junction leads to rapid cooling of the cladding layer in LR treatment. As shown in Figure 5(c), LR mainly affects the microstructure at the near-surface of the cladding layer, both the dendrite spacing and grains are reduced, which is also observed previously [12, 16, 17, 26]. In fact, during rapid heating and solidification of remelting, the temperature gradient at the molten pool surface is increased and the crystallization speed is accelerated, which results in refined dendrites along the solidification direction.

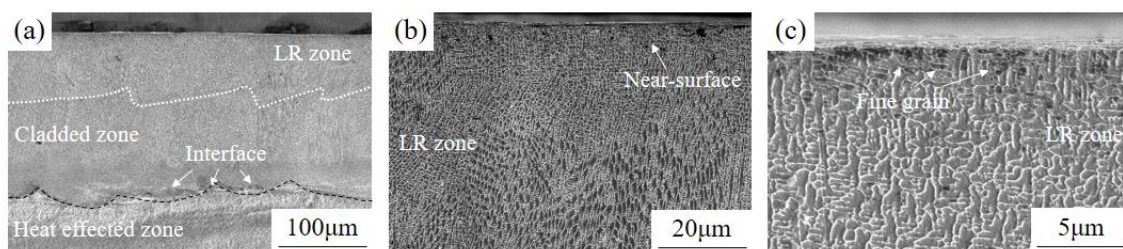


Figure 5. Near-surface SEM sectional morphologies of Ni-based alloy coatings via EHLA-LR: (a) overall morphology; (b) near-surface region; (c) dendrite morphology of near-surface region.

3.2 XRD Measurements

Figure 6 shows the XRD patterns of the EHLA and EHLA-LR specimens. The phase in the cladding layer is mainly consist of γ -(Ni, Fe) ductile phase, Cr_2Ni_3 phase, and a small amount of M_{23}C_6 hard phase, and change little before and after remelting. γ -(Ni, Fe) ductile phase has good plasticity and can alleviate the high hard brittleness caused by hard M_{23}C_6 phase. Cr_2Ni_3 phase is a Ni-rich phase, which is beneficial to improvement on the corrosion resistance of the cladding layer. The relative intensities of the diffraction peaks at 43.6° , 50.8° and 74.5° change from 5:10:1 to 4:7:1 after remelting, as a result of grain recrystallization. The similar phase change has been found and reported in Fe-based alloy coating by an integrated process of laser additive manufacturing and LR [16].

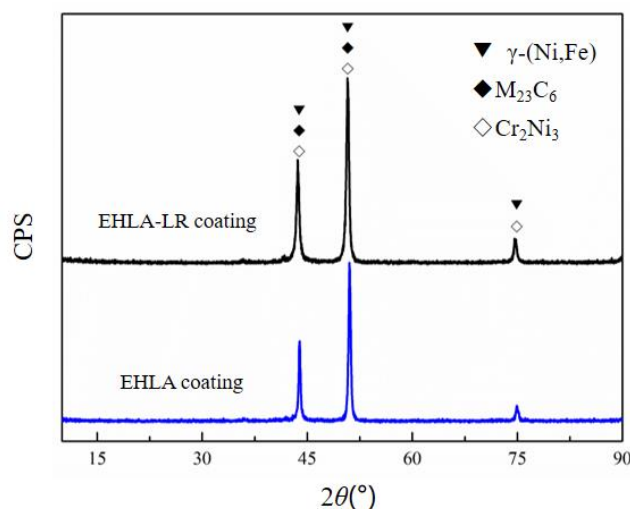


Figure 6. XRD spectra of Ni-based alloy coatings via EHLA and EHLA-LR.

3.3 Residual Stress Measurements

Figure 7 shows the shift of (220) diffraction peak of EHLA-LR specimen caused by lattice distortion at different Ψ angles. Accordingly, the residual stress is evaluated, and the results are displayed in Figure 8. The cladding coatings possess compressive stress no matter by laser remelting or not, but the residual compressive stress is slightly reduced upon LR. The compressive stress might be caused by the shrinkage at the near-surface quench zone, which could elongate the fatigue life of the cladding coatings.

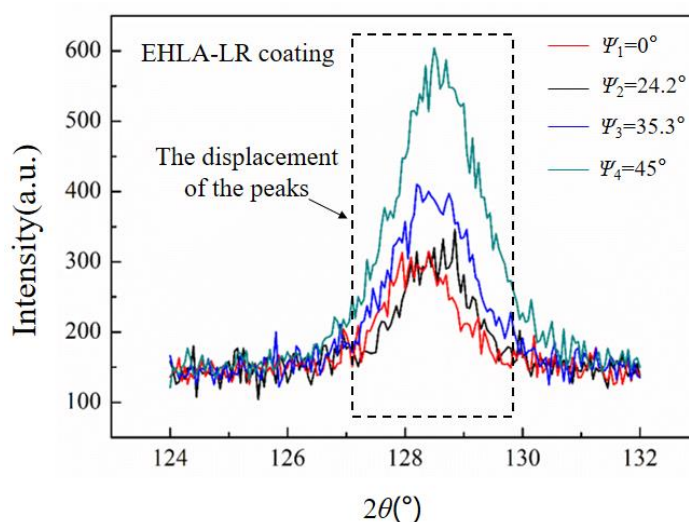


Figure 7. Diffraction peaks in high angle region of the Ni-based alloy coating via EHLA-LR in the residual stress measurements. The test is processed by the traditional $\sin^2\psi$ method with ψ of 0° , 24.2° , 35.3° and 45° . The (220) plane of the Ni-based alloy coatings is measured, corresponding to the 2θ and stress constant k of 128.78° and -675 MPa, respectively.

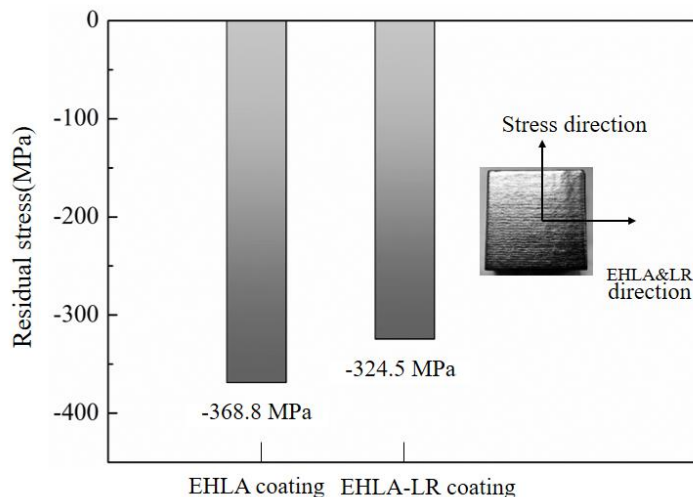


Figure 8. Results of residual stress in the surface of Ni-based alloy coatings. The illustration in the upper right corner of the figure shows the directions of the measured residual stress and the laser scanning processing.

3.4 Corrosion Resistance Experiments

Figure 9 shows the potential polarization curves of the substrate, the EHLA and EHLA-LR specimens. The coating via EHLA-LR has the highest self-corrosion potential E_{corr} of -0.432 V, which is considerably lower than that of 2Cr13 substrate (-0.675 V) and that of the specimen only via EHLA (-0.553 V), suggesting substantially enhanced corrosion resistance by LR treatment.

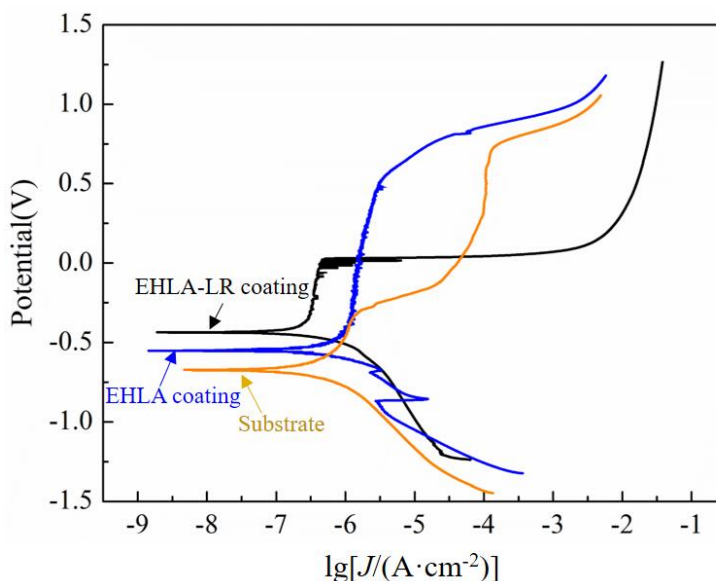


Figure 9. Potentiodynamic polarization curves of cladded Ni-based alloy coatings and 2Cr13 steel substrate in 3.5 wt% neutral NaCl solution at room temperature by electrochemical workstation (model CS350) with the scanning rate of 1 mV/s.

The fitting results of potentiodynamic polarization curves of clad Ni-based alloy coatings and 2Cr13 steel substrate are shown in Table 4. The lower the J_{corr} value is, the lower the corrosion rate of the EHLA-LR coating and the stronger the corrosion resistance. This can be ascribed to the increased surface compactness and refined microstructure in the coatings upon LR treatment. The improved corrosion resistance of the remelted Fe-based coatings was reported also by some investigators [16].

Table 4. Fitting results of potentiodynamic polarization curves of clad Ni-based alloy coatings and 2Cr13 steel substrate

Samples	E_{corr}/V	$J_{\text{corr}}/(\text{A} \cdot \text{cm}^{-2})$
EHLA-LR coating	-0.432	7.94×10^{-8}
EHLA coating	-0.553	8.91×10^{-8}
2Cr13 substrate	-0.675	2.29×10^{-7}

Figure 10 shows the morphology of the coatings before and after salt spray experiments, and Figure 11 shows the corrosion mass loss of the substrate, the EHLA and EHLA-LR specimens. The mass loss per unit area of 2Cr13 substrate is 2.166 mg, but is substantially reduced down to 0.127 mg after EHLA-LR process by 94.1%. Meanwhile, as shown in Figure 10(c), almost no corrosion products are evidenced on the coatings via EHLA-LR. The results demonstrate remarkably enhanced corrosion resistance of the coatings via EHLA-LR.

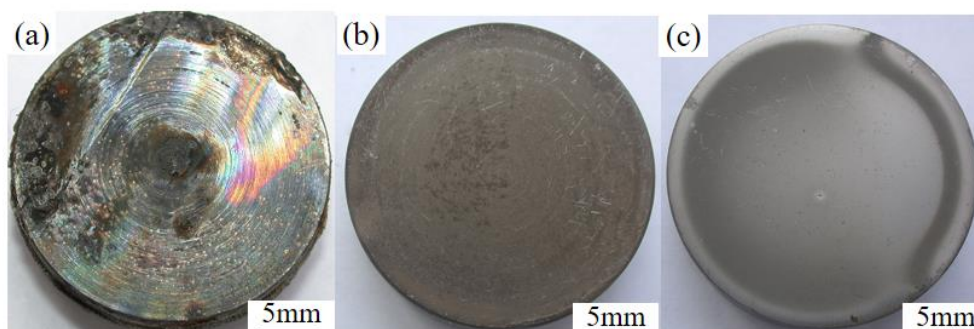


Figure 10. Comparison photos of sample surface morphologies after salt spray test in SHTH-270 salt spray test chamber at 35 °C for 96 h: (a) 2Cr13 steel substrate, (b) Ni-based alloy coating via EHLA; (c) Ni-based alloy coating via EHLA-LR.

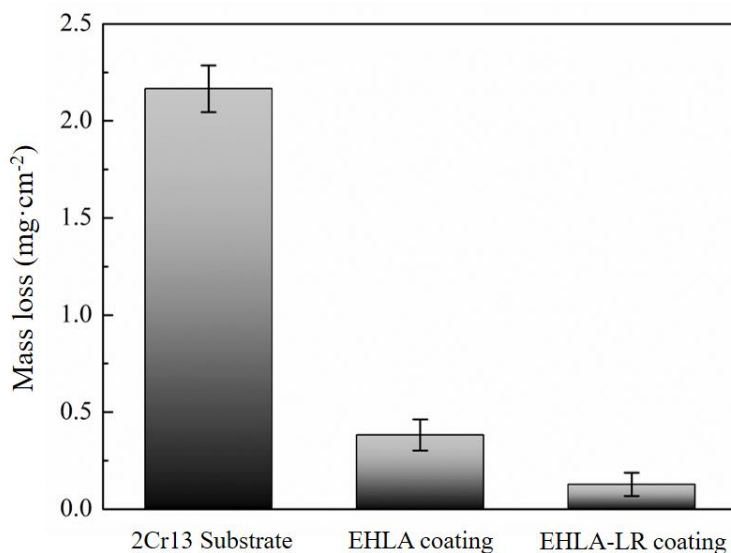


Figure 11. Mass loss per unit area of clad Ni-based alloy coatings and 2Cr13 steel substrate after salt spray test, with NaCl solution with PH value of 6.5 as the corrosive medium and immersion time of 96 h.

4. CONCLUSIONS

In order to improve the surface characteristics of the Ni-based coating produced by EHLA method, an integrated technology of EHLA-LR has been investigated in this research. In conclusion, LR could improve surface quality and corrosion resistance of Ni-based alloy coating fabricated using EHLA. LR treatment could lower the surface roughness and improve the surface compactness. Meanwhile, the spatters and un-melted powders on the coatings could be eliminated, and the dendrite spacing is reduced with refined grains in the near-surface region of the coatings. The coatings via EHLA are mainly composed of γ -(Ni, Fe), Cr_2Ni_3 and M_{23}C_6 , and change little upon LR treatment. The cladding coatings possess compressive stress, but the stress is slightly reduced via LR treatment. The coating via EHLA-LR has the self-corrosion potential E_{corr} higher than that of the substrate and the coatings via EHLA, and weight loss of the specimen via EHLA-LR after salt spray experiments is significantly reduced. Therefore, the corrosion resistance is substantially improved owing to the increased surface compactness and refined microstructure in the coatings. The integrated technology of EHLA-LR provides a potential method for preparing high quality Ni-based alloy coatings.

ACKNOWLEDGMENTS

The authors would like to express their gratitude for the financial support of the National Natural Science Foundation of China (Grant no. 52101097), the Natural Science Foundation of Shaanxi Province (Grant no. 2021JM-512, 2021JQ-797), the Science Foundation of Shaanxi Provincial Department of Education (21JS035), Xi'an Science and Technology Plan Project (2020KJWL01, 21XJZZ0069), the Youth Innovation Team of Shaanxi Universities, the research team of advanced surface engineering and equipment life extension of Xi'an University (XAWLK YTD013) and Tianyuan open fund of Shaanxi Key Laboratory of surface engineering and Remanufacturing (tywl2021-2).

References

1. L. Meng, P. H. Sheng, X. Y. Zeng, *J. Mater. Res. Technol.*, 16(2022)1732.
2. J. X. Yang, B. Bai, H. Ke, Z. Cui, Z. Liu, Z. Zhou, H. C. Xu, J. H. Xiao, Q. Liu, H. X. Li, *Opt. Laser. Technol.*, 144(2021)107431.
3. I. Kelbassa, A. Gasser, W. Meiners, G. Backes, B. Müller, High-speed LAM, *37th MATADOR Conference on Advanced Manufacturing*, The University of Manchester, Manchester, UK, 2012, 3386.
4. T. Schopphoven, A. Gasser, K. Wissenbach, *J. Laser. App.*, 28(2016)022501.
5. F. M. Shen, W. Tao, L. Q. Li, Y. D. Zhou, W. Wang, S. L. Wang, *Appl. Surf. Sci.*, 517(2020)146085.
6. Y. J. Li, S. Y. Dong, S. X. Yan, X. T. Liu, E. Z. Li, P. He, B. S. Xu, *Opt. Laser. Technol.*, 112(2019)30.
7. C. Kose, *Int. J. Electrochem. Sci.*, 11(2016)3542.
8. H. X. Chen, D. J. Kong, *Int. J. Electrochem. Sci.*, 13(2018)7800.
9. M. Vostřák, J. Tesař, Š. Houdková, E. Smazalová, M. Hruška, *Surf. Coat. Technol.*, 318(2017)360.
10. Š. Houdková, Z. Pala, E. Smazalová, M. Vostřáka, Z. Česánka, *Surf. Coat. Technol.*, 318(2017)129.
11. K. Yang, J. Q. Li, Q. Y. Wang, Z. Y. Li, Y. F. Jiang, Y. F. Bao, *Wear*, 426-427(2019)314.
12. P. Poza, C. J. Múnez, M. A. Garrido-Maneiro, S. Vezzù, S. Rech, A. Trentin, *Surf. Coat. Technol.*, 243(2014)51.
13. B. Das, M. Gopinath, A. K. Nath, P. P. Bandyopadhyay, *Optik*, 227(2021)166030.
14. H. Kawakami, H. Kuno, Y. Kawahito, H. Wang, *J. Mater. Process. Technol.*, 288(2021)116888.
15. D. P. Karmakar, G. Muvvala, A. K. Nath, *Surf. Coat. Technol.*, 422(2021)127498.
16. X. Xu, J. L. Du, K. Y. Luo, M. X. Peng, F. Xing, L. J. Wu, J. Z. Lu, *Surf. Coat. Technol.*, 422(2021)127500.
17. L.Y. Lou, C.X. Li, Y. Zhang, C.J. Li, H.F. Tian, F.L. Zhantai, *J. Yanshan. Univ.*, 44(2020)116.
18. D.W. Deng, Y.B. Ma, Y.S. Ma, T. He, Z.Y. Huang, Q. Sun, *Heat Treat. Met.*, 45(2020)113.
19. Q.M. Shi, G.Y. Zhong, Y. Sun, C. Politis, S.F. Yang, *J. Manuf. Process.*, 71(2021)345.
20. T.W. Hwang, S.W. Han, T. Lee, J.H. Kim, C.J.V. Tyne, Y.H. Moon, *J. Mater. Res. Technol.*, 9(2020)10447.
21. L.E. Paes, M. Pereira, F.A. Xavier, W.L. Weingaertner, L.O. Vilarinho, *J. Manuf. Process.*, 73(2022)67.
22. S. Kaierle, L. Overmeyer, I. Alfred, B. Rottwinkel, J. Hermsdorf, V. Wesling, N. Weidlich, *CIRP J. Manuf. Sci. Technol.*, 19(2017)196.
23. L. Chen, Y.Z. Sun, L. Li, Y.P. Ren, X.D. Ren, *Appl. Surf. Sci.*, 518(2020)145981.
24. Y. Wang, X. Chen, Q. Shen, C.C. Su, Y.P. Zhang, S. Jayalakshmi, R.A. Singh, *J. Manuf. Process.*, 64(2021)10.
25. Y.X. Qiao, J. Huang, D. Huang, J. Chen, W. Liu, Z.B. Wang, Z. Zhibin, *J. Chem.* 2020(2020)1438473.
26. J.C. Zhang, T.W. Huang, Z.L. Shen, H.J. Su, J. Zhang, L. Liu, *Mater. Lett.*, 304(2021)130710.